



# New insights into the inflamed tumor immune microenvironment of gastric cancer with lymphoid stroma: from morphology and digital analysis to gene expression

Irene Gullo<sup>1,2,3,4</sup> · Patrícia Oliveira<sup>3,4</sup> · Maria Athelougo<sup>5</sup> · Gilza Gonçalves<sup>2,3,4,6</sup> · Marta L. Pinto<sup>4,7,8</sup> · Joana Carvalho<sup>3,4</sup> · Ana Valente<sup>3,4</sup> · Hugo Pinheiro<sup>3,4,9</sup> · Sara Andrade<sup>3,4,10</sup> · Gabriela M. Almeida<sup>3,4</sup> · Ralf Huss<sup>5</sup> · Kakoli Das<sup>11</sup> · Patrick Tan<sup>11,12,13</sup> · José C. Machado<sup>2,3,4</sup> · Carla Oliveira<sup>2,3,4</sup> · Fátima Carneiro<sup>1,2,3,4</sup> 

Received: 16 April 2018 / Accepted: 9 May 2018 / Published online: 19 May 2018  
© The International Gastric Cancer Association and The Japanese Gastric Cancer Association 2018

## Abstract

**Background** Gastric cancer with lymphoid stroma (GCLS) is characterized by prominent stromal infiltration of T-lymphocytes. The aim of this study was to investigate GCLS biology through analysis of clinicopathological features, EBV infection, microsatellite instability (MSI), immune gene-expression profiling and PD-L1 status in neoplastic cells and tumor immune microenvironment.

**Methods** Twenty-four GCLSs were analyzed by RNA in situ hybridization for EBV (EBER), PCR/fragment analysis for MSI, immunohistochemistry (PD-L1, cytokeratin, CD3, CD8), co-immunofluorescence (CK/PD-L1, CD68/PD-L1), NanoString gene-expression assay for immune-related genes and *PD-L1* copy number alterations. CD3+ and CD8+ T-cell densities were calculated by digital analysis. Fifty-four non-GCLSs were used as control group.

**Results** GCLSs displayed distinctive clinicopathological features, such as lower pTNM stage ( $p=0.02$ ) and better overall survival ( $p=0.01$ ). EBV+ or MSI-high phenotype was found in 66.7 and 16.7% cases, respectively. GCLSs harbored a cytotoxic T-cell-inflamed profile, particularly at the invasive front of tumors ( $p<0.01$ ) and in EBV+ cases ( $p=0.01$ ). EBV+ GCLSs, when compared to EBV– GCLSs, showed higher mRNA expression of genes related to Th1/cytotoxic and immunosuppressive biomarkers. PD-L1 protein expression, observed in neoplastic and immune stromal cells (33.3 and 91.7%, respectively), and *PD-L1* amplification (18.8%) were restricted to EBV+/MSI-high tumors and correlated with high values of *PD-L1* mRNA expression.

**Conclusions** This study shows that GCLS has a distinctive clinico-pathological and molecular profile. Furthermore, through an in-depth study of tumor immune microenvironment—by digital analysis and mRNA expression profiling—it highlights the role of EBV infection in promoting an inflamed tumor microenvironment, with putative therapeutic implications.

**Keywords** Gastric cancer · Epstein–Barr virus (EBV) · Microsatellite instability (MSI) · Gene expression profiling · PD-L1

**Electronic supplementary material** The online version of this article (<https://doi.org/10.1007/s10120-018-0836-8>) contains supplementary material, which is available to authorized users.

✉ Carla Oliveira  
carlaol@ipatimup.pt

✉ Fátima Carneiro  
fcarneiro@ipatimup.pt

Extended author information available on the last page of the article

## Introduction

Gastric cancer (GC) represents a global health concern. It is the third leading cause of cancer mortality worldwide, with more than 720,000 estimated deaths in 2012 [1]. For patients with unresectable/metastatic disease, systemic chemotherapy may be the only therapeutic option, with objective response rates ranging from 20 to 40% and overall survival (OS) often less than 1 year [2, 3]. For these patients, targeted therapies have been approved, namely monoclonal antibodies targeting HER2 (trastuzumab) [4] and VEGFR2 [5, 6]. However, these therapies offer a limited survival advantage

(1.5–2.2 months) when compared to conventional chemotherapy alone [4–6].

Cancer immunotherapies, able to impair the cancer evasion from immune surveillance, have been explored as attractive therapeutic strategies for GC patients [7–9] and targeting of the PD-1/PD-L1 pathway has shown promising clinical results [9–11]. In September 2017, the Food and Drug Administration (FDA) approved the use of pembrolizumab (anti-PD-1 antibody) for the treatment of patients with recurrent, locally advanced, or metastatic gastric or gastroesophageal junction cancer (GC/EGJC), whose tumors express PD-L1 by immunohistochemistry (IHC) [12, 13]. Moreover, the FDA approved pembrolizumab for treating patients with unresectable or metastatic solid tumors, harboring microsatellite instability-high (MSI-high) status or DNA mismatch repair protein deficiency, regardless of tissue of origin or histotype [14].

GC is a heterogeneous disease, with several histological and molecular subtypes. However, effective stratification strategies and selection of predictive biomarkers for personalized medicine are currently limited [15]. Despite the recent advances in molecular research, the only predictive biomarkers approved for GC/EGJC include HER2 expression and/or gene amplification, for selecting patients eligible for trastuzumab treatment, and PD-L1 protein expression and/or MSI-high status for pembrolizumab immunotherapy, as stated above. Indeed, there is an urgent need to integrate clinical, morphological and molecular data for the stratification of patients for personalized therapy.

The Cancer Genome Atlas (TCGA) research network has proposed a four-tiered molecular classification, which identifies Epstein–Barr virus positive (EBV+), microsatellite unstable (MSI-high), genomically stable, and chromosomal unstable GCs [16]. Increasing evidence suggests promising results for the use of PD-1/PD-L1 blockade in patients bearing tumors classified as EBV+ and MSI-high [16–19]. Indeed, EBV infection and MSI-high status determine an increased burden of tumor neo-antigens and frequently drive a prominent infiltration of stromal immune cells within the tumor [20]. This explains the frequent association of these two molecular subtypes with the morphological features of GC with lymphoid stroma (GCLS) [21–24]. GCLS (alias medullary carcinoma, lymphoepithelioma-like carcinoma) was first reported by Watanabe et al. [25] and is recognized by the WHO classification as a rare histological variant of GC [26]. Strictly defined, GCLS shows the presence of a non-desmoplastic stroma “reminiscent of lymphoid tissue” [25], with prominent peri- and intra-tumoral infiltration of immune cells, mainly lymphocytes and plasma cells, uniformly present throughout the tumor, an expansive pattern of growth, and sparse aggregates of pleomorphic cancer cells, widely separated by the stromal elements of the tumors. Based on the assumption that PD-L1 immunoreactivity in

GC is related to high density of CD3+ and CD8+ tumor infiltrating lymphocytes (TILs) [27–30], as well as EBV+ and MSI-high molecular status [28, 31–33], an in-depth study of cases harboring GCLS morphology is of great interest.

Hence, the aim of this study was to characterize clinicopathological, immunohistochemical and molecular features of GCLS, with special attention to the immune context and well-recognized immunotherapy targets. Therefore, the specific objectives were: (1) studying GCLS biological behavior, through a detailed clinical and histopathological analysis; (2) examining the association between GCLS morphology and EBV+/MSI-high molecular status, in keeping with the TCGA molecular classification; (3) studying GCLS tumor immune microenvironment, by determining the density and topographic distribution of TILs and the mRNA expression of immune-related genes; (4) describing the PD-L1 status through detailed analysis of PD-L1 protein expression, *PD-L1* mRNA expression and copy number alterations (CNA).

## Materials and methods

### Patient series

Twenty-four GCs classified as GCLS, according to the 2010 World Health Organization (WHO) classification [26], were obtained retrospectively from the Department of Pathology of Centro Hospitalar São João (CHSJ). A tissue microarray (TMA) from 54 non-GCLS cases, stored in the Tumor Bank of CHSJ was used as control group. The clinicopathological features of the cases, collected from the files of the Department of Pathology and medical records were analyzed. None of the patients was submitted to neoadjuvant chemo- or radiotherapy. The study was approved by the Ethical Committee of the Hospital (CES 236-14).

### Immunohistochemistry (IHC) and EBV in situ hybridization (ISH)

Serial 3- $\mu$ m sections were prepared from one representative formalin-fixed paraffin-embedded (FFPE) block. IHC staining was performed in all GCLS cases with antibodies against cytokeratin (CK) AE1/AE3 (clone PCK26, prediluted; Ventana Medical Systems), CD3 (clone LN10, 1:500; Leica Biosystems), CD8 (clone SP57, prediluted; Ventana Medical Systems) and PD-L1 (clone E1L3N, 1:1000; Cell Signaling Technology) [17, 34, 35]. Samples were processed in the automatic Ventana Benchmark Ultra platform using the OptiView Universal DAB detection kit and the OptiView Amplification kit for PD-L1 staining. EBV infection was studied by chromogenic ISH for EBV-encoded

RNA (EBER-ISH, INFORM EBER probe, Ventana Medical Systems) using the same equipment, with enzymatic digestion (ISH protease) and the iViewBlue detection kit. Two TMA 3  $\mu\text{m}$  sections were prepared and used for PD-L1 IHC and EBER-ISH.

### Digital image analysis of CD3 and CD8 staining

Full thickness consecutive sections, stained for H&E, AE1/AE3, CD3 and CD8 were scanned with a 20 $\times$  objective, using the NanoZoomer 2.0HT virtual slide scanner (Hamamatsu Photonics). For each case the whole tumor area was selected, along with adjacent non-neoplastic mucosa and gastric wall, in the master slide stained for HE. Necrotic and ulcerated tissue was avoided. Using the Tissue Studio software (Tissue Phenomics Technology, Definiens), the tumor center (TC) and the invasive front (IF) were selected and segmented for each virtual slide. The consecutive stainings were co-registered (i.e. superimposed) to evaluate the correlation of the different biomarkers in corresponding areas. The percentage of positive staining within the TC and the IF was measured automatically using the Tissue Studio and Definiens Developer softwares, which allow the automatic detection, segmentation and classification of positive and negative cells. Using this image analysis platform, CD3 and CD8 T cells density were calculated both in the TC, at the IF and in the whole tumor.

### Evaluation of PD-L1 expression

In GCLSs, PD-L1 immunoexpression was evaluated for tumor epithelial and stromal immune cells (IG, FC). A semi-quantitative evaluation was performed, using the immunoreactivity scoring system (IRS) recently described by Boger et al. [34] in a study using the same anti-PD-L1 clone. PD-L1 expression in tumor epithelial cells was dichotomized as positive or negative by an immunoreactivity score (IRS) of 2. A 1% threshold of PD-L1 expression in stromal immune cells was defined as positive. In the evaluation of the TMA, two separate cores of each tumor were analyzed.

### PD-L1/CK and PD-L1/CD68 double immunofluorescence

To explore the differential expression of PD-L1 in tumor epithelial cells versus stromal immune cells five GCLS cases, with an IRS  $\geq 7$ , were double stained for PD-L1/CK and PD-L1/CD68 (clone PG-M1, 1:100; Dako Agilent Technologies). The antigen retrieval was performed using the automatic Ventana Benchmark Ultra platform, while the following steps were performed manually. Briefly, slides were incubated with 0.1% Sudan Black B in 70% ethanol and Ultra V Block (Lab Vision, Thermo Fisher Scientific) to

reduce tissue autofluorescence and non-specific background staining. After primary antibody incubation, a combination of donkey anti-rabbit biotinylated antibody (1:250; Novex, Thermo Fisher Scientific) and donkey anti-mouse conjugated with Alexa Fluor 647 antibody (1:200; Invitrogen, Thermo Fisher Scientific) was applied, followed by incubation with streptavidin conjugated with Alexa Fluor 555 antibody (1:500; Invitrogen, Thermo Fisher Scientific). Finally, slides were counterstained with Vectashield containing DAPI (Vector Laboratories) and visualized using a Zeiss AxioImager Z1 microscope (Carl Zeiss MicroImaging).

### DNA and RNA extraction

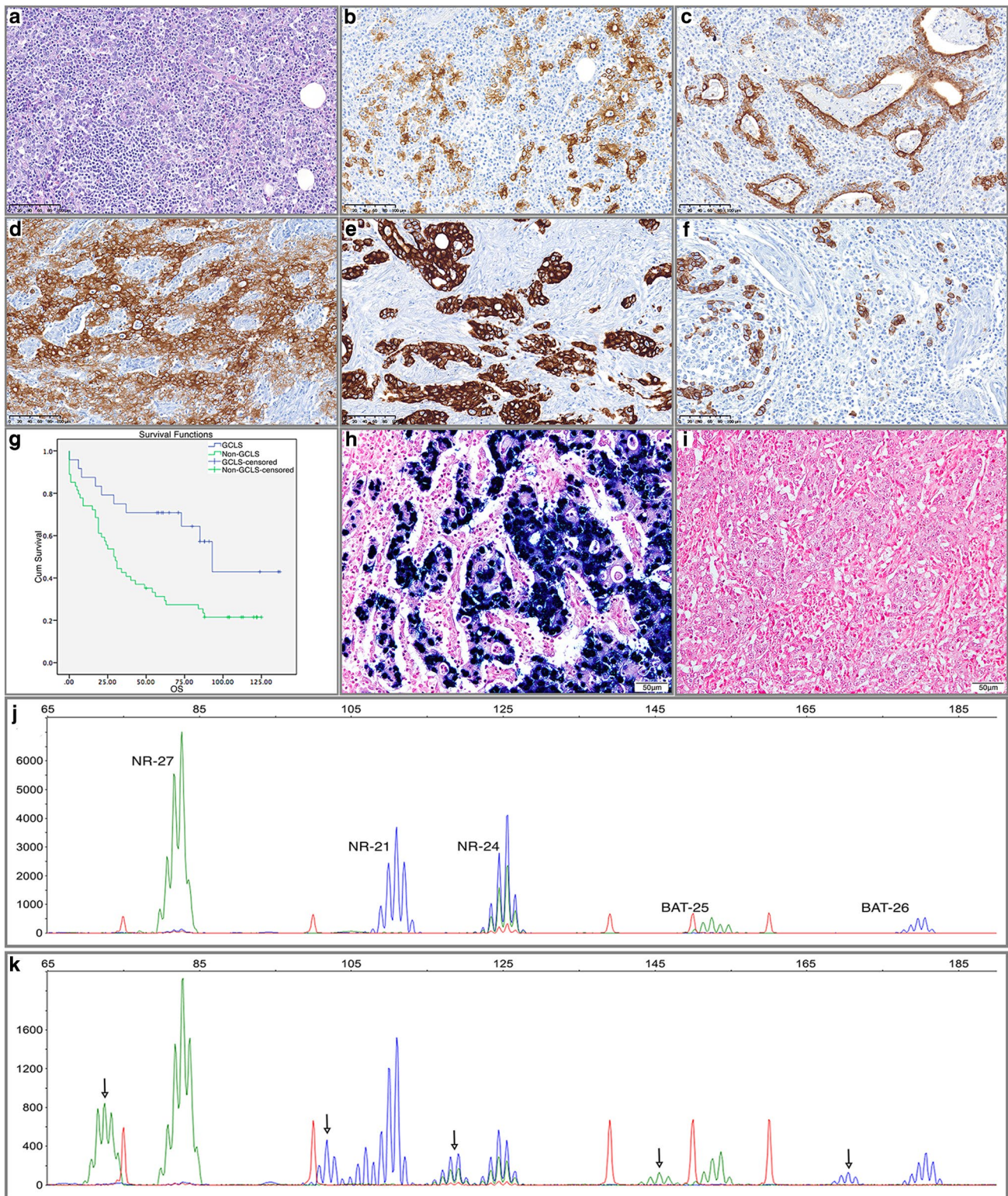
Genomic DNA and total RNA of GCLS cases was extracted from FFPE tissues (four sections, each 10  $\mu\text{m}$  thick) using QIAamp DNA Mini Kit and miRNeasy Mini Kit (Qiagen, Valencia, CA), respectively, in accordance with the manufacturer's instructions. Before extraction, tissue sections were manually microdissected to ensure high tumor content. DNA purity and quantification and RNA concentrations were assessed using the NanoDrop 2000 UV-Vis spectrophotometer (NanoDrop products, Wilmington, DE).

### Study of MSI phenotype and PD-L1 CNAs

DNA isolated from FFPE tissues was analyzed for the presence of MSI phenotype and *PD-L1* CNA by polymerase chain reaction (PCR). Five mononucleotide markers (BAT-25, BAT-26, NR-24, NR-21 and NR-27) were used as a pentaplex panel to determine MSI phenotype (Multiplex PCR, Qiagen). Tumors with instability involving at least two of the five *loci* were classified as MSI. The MSI status of 23 cases from the TMA group had been previously characterized using the same pentaplex panel (Qiagen). *PD-L1* CNAs were examined by quantitative real-time PCR using a Taqman copy number assay (*PD-L1*: ID Hs00268713\_cn) and a TaqMan Copy Number Reference Assay (Human, RNase P: ID4403326), both obtained from Thermo Fisher Scientific.

### NanoString quantification and analysis

A NanoString nCounter CodeSet was designed, comprising custom-designed probes of 100-bp targeting 474 genes previously published [36] and several additional genes associated with immune response (*CCL22*, *CCR7*, *CD3D*, *CD3E*, *CD3G*, *CD8A*, *CD8B*, *CD19*, *CD20*, *CD45*, *CD68*, *CXCL10*, *CXCL11*, *FOXP3*, *GZMA*, *GZMB*, *IL4*, *IL13*, *PD1*, *PD-L1*, *TNFA*). Analysis and normalization of the raw NanoString data was conducted using the nSolver Analysis Software v2.0, using all positive, negative controls and housekeeping probes, according to the manufacturer's protocol



(NanoString Technologies). Normalized data were log<sub>2</sub>-transformed. Individual genes related to immune response were selected for further analyses and a heatmap illustrating Z-score scaled values for EBV+ and EBV- samples was generated using the R package “gplots” [37].

### Statistical analysis

IBM SPSS (Release 20.0.0) and SigmaPlot (Systat Software 11.0) were used for statistical analysis. All tests were two-sided, and differences were considered significant

**Fig. 1** Histopathological and molecular features of GCLS. The inflammatory infiltrate of GCLS is so abundant that may obscure tumor epithelial cells (**a**, HE  $\times 200$  original magnification). These can be highlighted by cytokeratin immunostaining (**b**, CK AE1/AE3 original magnification  $\times 200$ ). GCLS showed heterogeneous architectural patterns: the neoplastic cells were arranged in tubules (**c**), lace-like pattern (**d**), trabeculae/cords and cribriform structures (**e**) or even isolated cells (**f**) (CK AE1/AE3 original magnification  $\times 200$ ). Overall survival (OS) analysis, stratified by GCLS morphology, demonstrated that GCLS cases presented better OS compared to non-GCLS cases (Kaplan–Meier curve,  $p=0.01$ ) (**g**). EBV infection was determined by EBER-ISH that allowed the direct visualization of positive (**h**) or negative (**i**) probe signals in cancer-infected cells. MSI phenotype was determined by fluorescent pentaplex PCR using a panel of five mononucleotide markers (NR-27, NR-21, NR-24, BAT-25, BAT-26) (**j**, **k**). The EBV+ case (**h**) was MSS (**j**), whereas the EBV– case (**i**) was MSI-high, with additional alleles in five of five mononucleotide microsatellite loci (**k**, arrows)

when  $p < 0.05$ . Comparisons of categorical variables were performed by Chi square test or Fisher's exact test, as appropriate. A Spearman's rank-order correlation was run to determine the relationship between PD-L1 protein expression and *PD-L1* gene expression levels. Comparisons of quantitative variables were performed by Student *t* test and Mann–Whitney/Wilcoxon test, as appropriate. OS was defined as the duration (months) from the date of surgery until death from any cause. Patients who were alive were censored at the last follow-up date. OS rates were estimated using the Kaplan–Meier method. Hazard ratios of variables were calculated by univariate Cox regression and those having  $p$  values up to 0.01 were included in a multivariate Cox regression, to identify independent prognostic variables.

## Results

### GCLS has distinctive clinicopathological features

All cases were characterized by a prominent lymphoid infiltration of the stroma and fulfill the morphological criteria defining GCLS morphology [26]. Often the lymphoid infiltrate was so prominent that CK immunostaining was necessary to identify the cancer epithelial cells and to define the tumor structure (Fig. 1a, b). Tumor cells showed heterogeneous architectural patterns (Fig. 1c–f) and were arranged in tubules, cords/trabeculae, nests or isolated cells. Specific patterns were observed in some areas, such as lace-like, cribriform or microglandular structures. The immune infiltrate was predominantly constituted by lymphocytes and plasma cells, with frequent lymphoid follicles in the TC and/or at the IF (13/24, 54.2%). Macrophages, eosinophils and neutrophils were also intermingled, and mucosal ulceration was frequently observed (10/24, 41.7%).

By comparison with non-GCLS cases, GCLSs were characterized by distinctive clinicopathological features

(Table 1): younger age ( $p=0.03$ ), upper location ( $p=0.04$ ), expansive pattern of growth ( $p < 0.01$ ), less advanced pTNM stage ( $p < 0.01$ ), lower frequency of lymph node metastasis ( $p=0.01$ ), lymphatic invasion ( $p=0.02$ ) and distant metastasis ( $p=0.02$ ) and better OS ( $p=0.01$ ) (Fig. 1g). By multivariate analysis, only the absence of distant metastases remained in the Cox regression model as an independent good prognostic factor.

### GCLS is associated with a high rate of EBV infection

To investigate the relationship between GCLS morphology and EBV infection and MSI status, we searched for EBV infection by EBER in situ hybridization (EBER-ISH) and for MSI by multiplex PCR.

In the series of 24 GCLSs, 16 cases were EBV+/MSS (66.7%), 4 were EBV–/MSI-high (16.7%) and 4 cases were EBV–/MSS (16.7%) (Fig. 1h–k). Not a single case was typed as EBV+/MSI-high. In EBV+ cases, positive EBER-ISH probe signals were found in virtually all cancer cells and, in some of them, in scattered lymphocytes of the non-neoplastic mucosa.

By comparison with non-GCLS cases, GCLS cases were characterized by higher frequency of EBV infection (66.7 vs 5.6%,  $p < 0.01$ ) (Table 1). No statistically significant difference was found between GCLS and non-GCLS cases regarding MSI status (16.7 vs 27.8%,  $p=0.29$ ).

### Insights into the tumor microenvironment: GCLS is characterized by a Th1/cytotoxic inflamed phenotype

To characterize the immune infiltrate in GCLS cases, we quantified CD3+ and CD8+ T-cell densities, using a dedicated digital analysis platform (Definiens®). The analysis was possible in 20/24 cases [EBV+ ( $n=12$ ) and EBV– GCLSs ( $n=8$ )]. The specific objectives were to analyze the spatial distribution in the TC and at the IF and to investigate the relationship with EBV infection. Moreover, we analyzed, in 23/24 cases [EBV+ ( $n=15$ ), EBV– GCLSs ( $n=8$ )], mRNA expression levels of several immune-related genes selected from a broader gene expression panel obtained through Nanostring technology, to characterize the type of immune response and to investigate possible relationships with EBV+ and MSI-high molecular subtypes.

Regarding spatial distribution, T-cell density was higher at the IF compared to the TC (Fig. 2a–d, Tab. S1), both for CD3+ T cells ( $p=0.013$ ) and CD8+ T cells ( $p < 0.01$ ), regardless of the EBV status. When compared with EBV– cases ( $n=8$ ), EBV+ GCLS cases ( $n=12$ ) showed a significantly higher number of CD3+ T cells ( $p < 0.01$ ) and CD8+ T cells ( $p=0.01$ ), as calculated in the whole tumor (Fig. 2e, f, Tab. S1). These results were confirmed by mRNA

**Table 1** Clinicopathological features, EBV infection, MSI status and PD-L1 expression of GCLS compared to non-GCLS cases

Feature	GCLS (n=24)	Non-GCLS (n=54)	p value
Gender			
Male	17/24 (70.8%)	28/54 (51.9%)	0.12
Female	7/24 (29.2%)	26/54 (48.1%)	
Age (years)			
≤60	9/24 (37.5%)	8/54 (14.8%)	0.03*
>60	15/24 (62.5%)	46/54 (85.2%)	
Location			
Antrum	10/24 (41.7%)	35/53 (66%)	0.04*
Non-antrum	14/24 (58.3%) <sup>a</sup>	18/53 (34.0%)	
Size			
<5 cm	8/24 (33.3%)	15/54 (27.8%)	0.62
≥5 cm	16/24 (66.7%)	39/54 (72.2%)	
Pattern of growth			
Infiltrative	9/24 (37.5%)	41/52 (78.8%)	<0.001*
Expansive	15/24 (62.5%)	11/52 (21.2%)	
Lymphatic invasion			
L0	9/24 (37.5%)	7/54 (13.0%)	0.02*
L1	15/24 (62.5%)	47/54 (87.0%)	
Venous invasion			
V0	11/24 (45.8%)	15/54 (27.8%)	0.12
V1	13/24 (54.2%)	39/54 (72.2%)	
Perineural invasion			
P0	14/24 (58.3%)	18/53 (34.0%)	0.04*
P1	10/24 (41.7%)	35/53 (66.0%)	
pT category			
pT1 or pT2	6/24 (25.0%)	27/54 (50.0%)	0.04*
pT3 or pT4	18/24 (75.0%)	27/54 (50.0%)	
pN category			
No lymph node metastasis	9/24 (37.5%)	6/54 (11.1%)	0.01*
Lymph node metastasis	15/24 (62.5%)	48/54 (88.9%)	
M category			
M0	23/24 (95.8%)	47/54 (87.0%)	0.02*
M1	1/24 (4.2%)	7/54 (13.0%)	
TNM stage			
IA, IB	6/24 (25%)	7/54 (13.0%)	0.002*
IIA, IIB	11/24 (45.8%)	8/54 (14.8%)	
IIIA, IIIB, IIIC	6/24 (25%)	24/54 (44.4%)	
IV	1/24 (4.2%)	15/54 (27.8%)	
Overall survival			
Median survival (months)	93.0	29.0	0.01*
95% CI	76.47–109.53	20.60–37.4	
EBV infection			
Positive	16/24 (66.7%)	3/54 (5.6%)	<0.001*
Negative	8/24 (33.3%)	51/54 (94.4%)	
MSI status			
MSS	20/24 (83.3%)	39/54 (72.2%)	0.29
MSI	4/24 (16.7%)	15/54 (27.8%)	
PD-L1			
Negative	16/24 (66.7%)	47/54 (87.0%)	0.04*
Positive	8/24 (33.3%)	7/54 (13.0%)	

Cases were staged according to the TNM system—8th edition (AJCC)

Statistical significant results ( $p < 0.05$ ) are marked with an asterisk (\*)

<sup>a</sup>Three GCLSs (12.5%) developed in gastric stump after previous distal gastrectomy

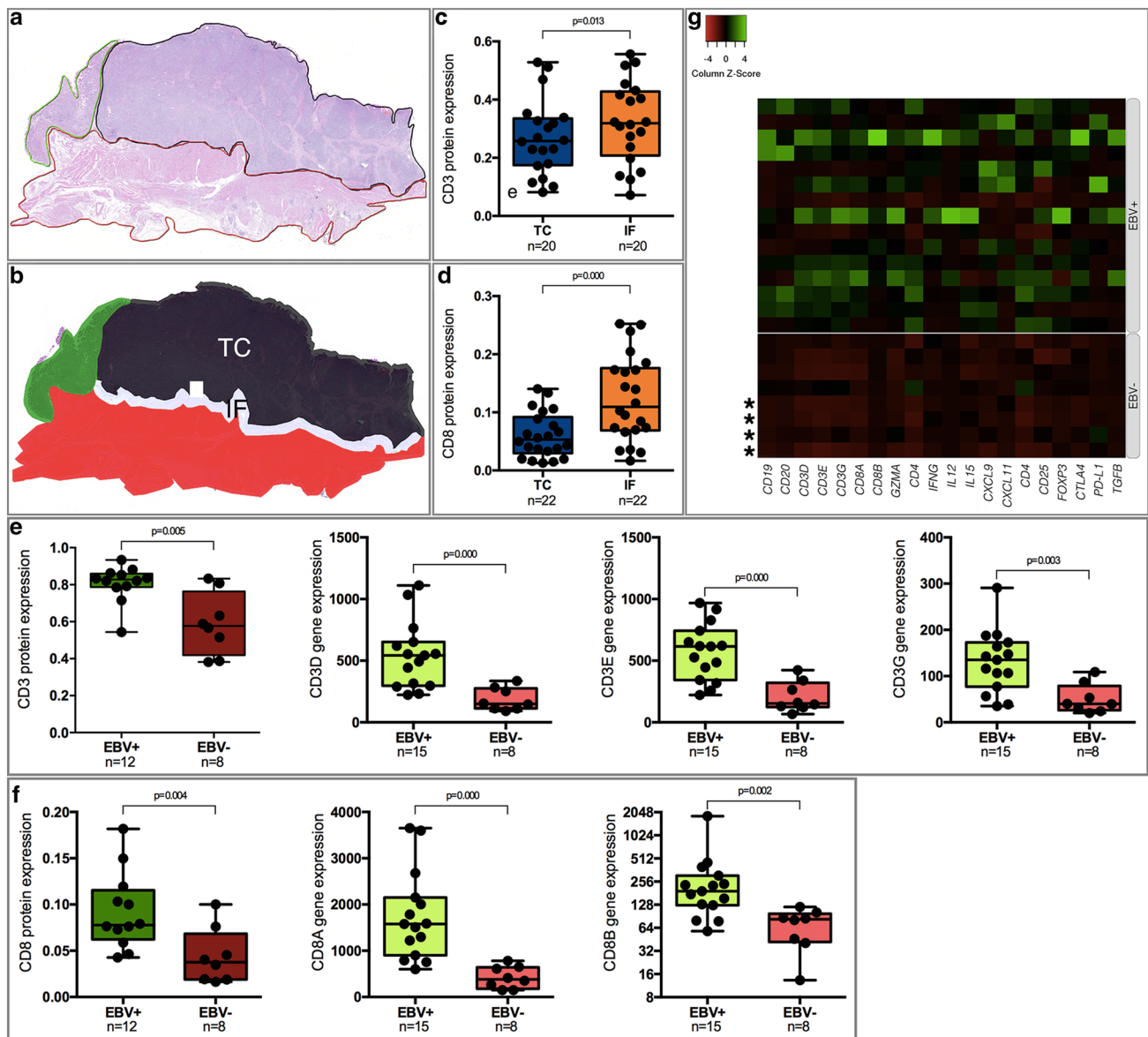


**Fig. 2** Characterization of tumor immune microenvironment in GCLS cases. The whole tumor area (black), the adjacent non-neoplastic mucosa (green) and the gastric wall (red) were annotated in the master slide stained for HE (**a**, **b**). Using the Tissue Studio software, the tumor center (TC) and the invasive front (IF) of the tumor were selected and segmented (**b**). Digital spatial analysis (Tissue Studio and Definiens Developer systems) of CD3+ and CD8+ T cells revealed that CD3 (**c**) and CD8 (**d**) T cells were more abundant at the IF compared to the TC. The analysis of lymphocytic infiltrates

in EBV+ and EBV- GCLSs revealed that CD3+ (**e**) and CD8+ (**f**) T cells were more abundant in EBV+ GCLSs compared to EBV- GCLSs, as demonstrated by protein (left panel) and mRNA expression (right panels). The heatmap **g** shows differential expression of immune-related genes in EBV+ and EBV- GCLSs. EBV+ GCLSs were characterized by an inflamed T-cell phenotype with high expression of biomarkers of regulatory T cells and immune inhibitory checkpoints. Cases harboring MSI-high molecular status are marked with an asterisk

expression analysis of CD3 (*CD3D*, *CD3E*, *CD3G*) and CD8 (*CD8A* and *CD8B*) transcripts (Fig. 2e, f, Tab. S2).

Immune-related genes mRNA expression profiling of EBV+ (*n* = 15), compared to EBV- GCLSs (*n* = 8), revealed an up-regulation of genes related to B-cell (*CD19*, *CD20*) and T-cell (*CD3D*, *CD3E*, *CD3G*) response. A more in-depth characterization of T-cell profile showed,

in EBV+ GCLSs, enrichment of genes related to cytotoxic T cells, Th1 cells and pro-inflammatory factors (*CD8A*, *CD8B*, *GZMA*, *CD4*, *IFNG*, *IL12*, *IL15*, *CXCL9*, *CXCL10*), along with genes indicative of activation of regulatory T cells and immune inhibitory checkpoints (*CD4*, *CD25*, *FOXP3*, *CTLA4*, *PD-L1*, *TGFB*) (Fig. 2g, Tab. S2).

In summary, GCLS cases were characterized by an inflamed tumor microenvironment, enriched in T lymphocytes, particularly at the IF of the tumors and in EBV+ cases. Digital analysis quantification of TILs and mRNA expression profiling of immune-related genes revealed that, within GCLSs, the molecular subgroup of EBV+ tumors showed the most striking T-cell inflamed phenotype, with the highest expression of negative regulatory factors.

### PD-L1-positive status is a frequent finding in GCLS and is restricted to EBV+ and MSI-high molecular subtypes

In view of the results obtained by mRNA expression profiling of immune-related genes and based on the evidence that the tumor immune-inflamed phenotype correlates generally with higher response rates to anti-PD-L1/PD-1 therapy [38], we decided to further characterize GCLS by investigating PD-L1 protein expression and *PD-L1* copy number alterations.

In our GCLS series, PD-L1 protein expression was observed in cancer and stromal immune cells, but not in non-neoplastic epithelium. Strong PD-L1 immunoreactivity, predominantly membranous (complete or partial), was observed in tumor epithelial cells, whereas cytoplasmic, granular and dotted staining patterns were observed in stromal immune cells (Fig. 3a–c). PD-L1 immunoreactivity was observed at the cell membrane of tumor epithelial cells (IRS > 2) in 8/24 GCLSs (33.3%) and in stromal immune cells ( $\geq 1\%$ ) in 22/24 GCLSs (91.7%) (Table 2).

There was a positive correlation between PD-L1 protein expression in tumor cells, calculated by IRS, and *PD-L1* gene expression ( $r_s = 0.622$ ,  $p < 0.01$ ). Indeed, high PD-L1 protein immunoreactivity corresponded generally to high *PD-L1* mRNA levels (Fig. 3d, Tab. S3). One outlier case was identified, with the highest value of protein immunoreactivity (IRS = 7) and low mRNA value, which might be explained by the high intra-tumor heterogeneity of PD-L1 protein expression found in this particular case (Fig. S1).

PD-L1 positive immunoreactivity, dichotomized by an IRS > 2 and *PD-L1* high gene expression, defined by the median value of expression, were restricted to EBV+ (37.5 and 62.5%, respectively) and MSI-high (50% for both parameters) GCLSs (Tab. S3).

To further elucidate whether PD-L1 was localized not only in cancer cells, but also in CD68+ stromal immune cells, we performed double immunofluorescence for PD-L1/CK and PD-L1/CD68 in all cases with IRS  $\geq 7$  ( $n = 5$ ). We verified that PD-L1 immunoreactivity was co-localized both in CK+ cancer cells and CD68+ stromal immune cells (Fig. 3e, f).

When compared with non-GCLS cases, the GCLSs series was characterized by higher frequency of PD-L1

immunoexpression (33.3 vs 13.0%,  $p = 0.04$ ) (Table 1). In non-GCLS cases, PD-L1 immunoreactivity was also observed at the cell membrane of tumor epithelial cells and in stromal immune cells.

To comprehensively characterize PD-L1 status in GCLS, we also analyzed *PD-L1* CNAs by real-time PCR (Taqman copy number assay), aiming to investigate if PD-L1 expression in GCLS was driven by gene amplification.

We were able to retrieve consistent results for *PD-L1* CNAs in 16/24 cases. From these, 3/16 (18.8%) cases harbored *PD-L1* amplification (three copies), 10/16 (62.5%) showed a normal *PD-L1* status (two copies), and 3/16 (18.8%) displayed *PD-L1* loss of heterozygosity (LOH, one copy) (Tab. S3).

All cases harboring *PD-L1* amplification showed high levels of *PD-L1* gene expression [median value = 166.48 (amplified), 26.26 (normal) and 9.79 (LOH),  $p = 0.024$ ] and high PD-L1 protein immunoreactivity in tumor and stromal immune cells (Fig. 3d, Tab. S3). Noteworthy, two cases were EBV+ and one case presented MSI-high status (Tab. S3).

Among the 13 cases with either normal *PD-L1* status ( $n = 10$ ) or LOH ( $n = 3$ ), three cases exhibited high PD-L1 protein expression in cancer cells, suggesting that alternative genetic/epigenetic mechanisms could be driving PD-L1 overexpression besides gene amplification.

In summary, as determined by protein and mRNA expression analysis, GCLS showed frequently PD-L1 positive status, which was restricted to EBV+ and MSI-high tumors.

## Discussion

The aim of this study was to analyze the clinicopathological and molecular profile of GCLS, with special focus on EBV infection, MSI status, tumor immune microenvironment and PD-L1 status.

GCLS is a rare variant of GC (1–4%) [25] with distinctive biological characteristics. As verified in this study, the majority of patients diagnosed with GCLS presents with less advanced disease and has good prognostic outcomes [25, 39–41]. The high density of lymphocytic infiltrate, along with the distribution and the functional orientation of immune cells characterizing GCLS, as described in this study, might explain, at least in part, the favorable clinical behavior of this tumor type [42].

Our results are in keeping with those in the literature that describe, in GCLS cases, rates of EBV infection varying from 31 to 100% and MSI-high status restricted to non-EBV GCLS [23, 40, 43, 44]. Indeed, EBV infection and MSI-high status are mutually exclusive events in GC. It has been suggested that they represent two alternative pathways of gastric carcinogenesis that have in common a high immune response, driven by the immunogenicity

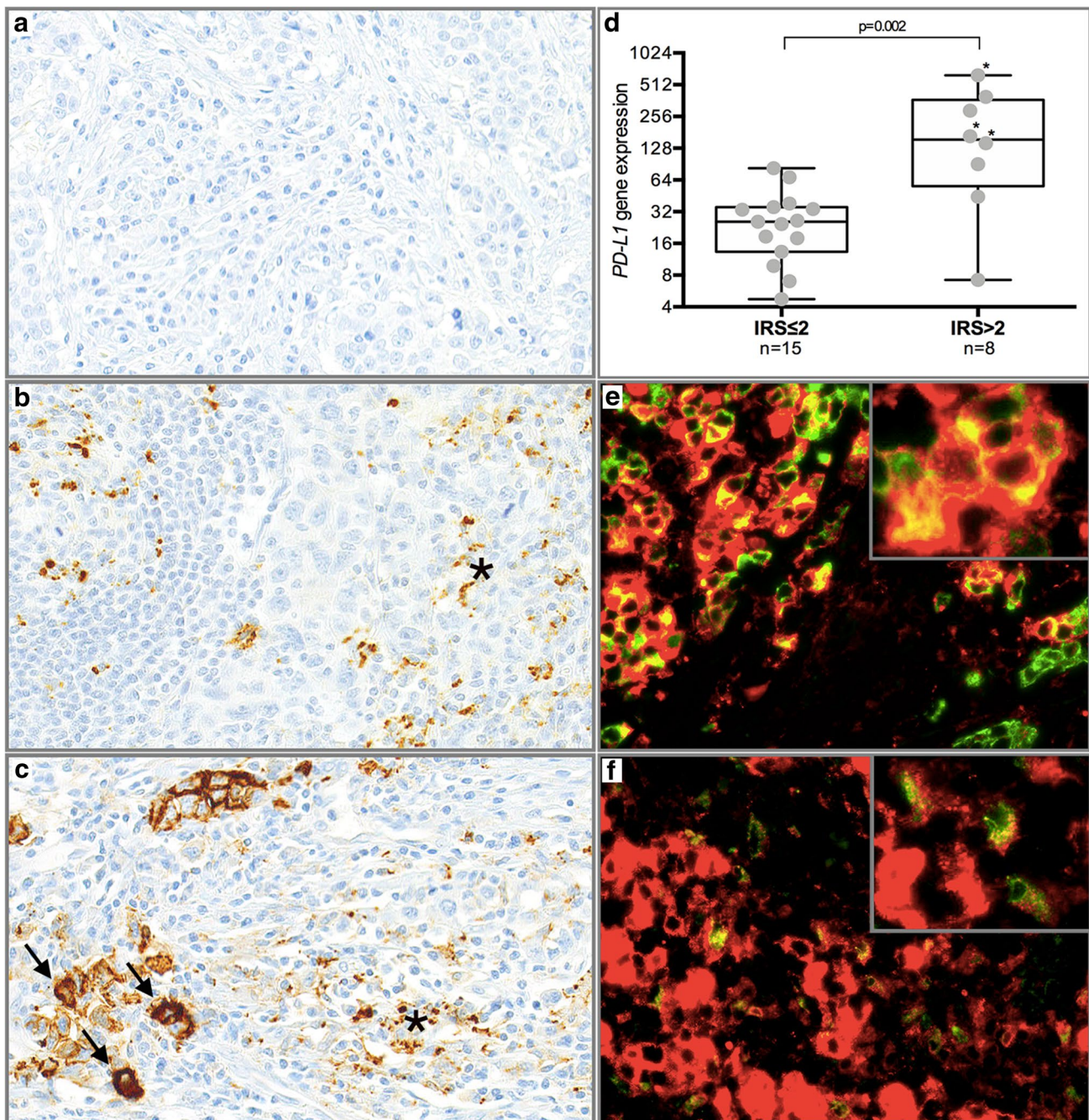


**Fig. 3** PD-L1 status in GCLS. PD-L1 expression was absent (a), positive in stromal immune cells (b) or positive in cancer and stromal immune cells (c) (PD-L1 IHC,  $\times 200$  original magnification). Lymphoid follicles, with PD-L1+ cells inside the germinal center (b, left) served as internal positive control. Membranous, linear and strong PD-L1 expression was observed in cancer cells (c, arrows), whereas cytoplasmic dotted/granular pattern was observed in stromal immune

cells (b, c, asterisk). A positive correlation was found between *PD-L1* mRNA expression and PD-L1 protein expression (d):  $r_s = 0.622$ ,  $p = 0.002$ ; median value = 25.66 (IRS  $\leq 2$ ), 154.55 (IRS  $> 2$ ). Cases marked with an asterisk showed *PD-L1* gene amplification. Double immunofluorescence for PD-L1 (red) and CK (green) (e) and PD-L1 (red) and CD68 (green) (f) showed PD-L1 co-localization both in neoplastic cells (e) and stromal immune cells (f)

of viral and mutation-associated neoantigens [19, 21, 45, 46]. In this study, the presence of EBV infection was significantly higher in GCLS cases (66.7%), compared with cases lacking a GCLS phenotype (5.6%). Accordingly, the

recognition of GCLS morphological features is useful for the molecular stratification of GC and should prompt a search for EBV infection. In contrast, GCLS cases showed lower frequency of MSI-high status (16.7%), compared to

**Table 2** PD-L1 expression in tumor epithelial and stromal immune cells in GCLS

PD-L1 expression in tumor epithelial cells	N (%)
<b>PD-L1 quantity score (A)</b>	
0 (0%)	14 (58.3)
1 ( $\leq 1\%$ )	2 (8.3)
2 (2–10%)	1 (4.2)
3 (11–50%)	2 (8.3)
4 ( $> 50\%$ )	5 (20.8)
<b>PD-L1 intensity score (B)</b>	
0 (negative)	14 (58.3)
1 (weak)	2 (8.3)
2 (medium)	0 (0.0)
3 (strong)	8 (33.3)
<b>Immunoreactivity score (IRS = A + B)</b>	
0	14 (58.3)
2	2 (8.3)
3	0 (0.0)
4	0 (0.0)
5	1 (4.2)
6	2 (8.3)
7	5 (20.8)
<b>PD-L1 status (dichotomisation by IRS of 2)</b>	
Positive (IRS $> 2$ )	8 (33.3)
Negative (IRS $\leq 2$ )	16 (66.7)
<b>PD-L1 expression in stromal immune cells</b>	
0 (0%)	2 (8.3)
1 (1–5%)	7 (29.2)
2 (6–20%)	9 (37.5)
3 ( $> 20\%$ )	6 (25.0)

the non-GCLS group (27.8%). This discrepancy might be biased by the high number of EBV infected GCLS (66.7%) and the mutual exclusivity of the EBV+ and MSI-high molecular subtypes.

A detailed characterization of the immune infiltrate of GCLS is still lacking and has been explored in depth in this study.

Tumors can be classified into different cancer-immune profiles, including “inflamed” and “non-inflamed” (immune-deserts or immune-excluded) phenotypes [38]. “Inflamed” tumors show a pre-existing anti-tumor immune response that has been inhibited, including dense CD8+ T-cell infiltrates within the whole tumor, a broad pro-inflammatory cytokine profile, a type I interferon (IFN) signature and high levels of PD-L1 expression on immune, or even cancer cells [38]. In contrast, the “non-inflamed” phenotype lacks the above features. This classification has potential practical implications to guide immunotherapy strategies: clinical responses to anti-PD-1/PD-L1 therapy occur more frequently in patients harboring tumors with an inflamed phenotype [38].

With the support of digital analysis of immune biomarkers and mRNA expression analysis, in this study we were able to demonstrate that the majority of GCLS cases show immune characteristics of “inflamed” tumors. Moreover, high PD-L1 protein expression, both in cancer and immune cells infiltrating the tumor microenvironment, and *PD-L1* gene expression are frequent in these tumors, specifically in EBV+ and MSI-high molecular subtypes. Taken together, these results suggest that PD-1/PD-L1 pathway is a critical molecular mechanism in GCLS that could be exploited for targeted immunotherapy.

In this study, we also analyzed mRNA expression profiling of immune-related genes by comparing EBV+ and EBV– GCLS cases. Even in the context of the same immune-rich tumor microenvironment, i.e. the presence of GCLS morphological features, EBV+ GCLSs showed a distinctive immunological mRNA profile: they were enriched in genes related to T-cell differentiation, cytotoxic function, pro-inflammatory cytokines/chemokines, including IFN $\gamma$  response, and genes of the immune checkpoint inhibitor pathways (*CTLA4*, *PD-L1*). Similar results have been observed in previous studies, on the basis of TCGA transcriptomic data [31, 47, 48]. Moreover, these results, concerning mRNA data, were confirmed at the protein level: digital analysis of CD3 and CD8 protein expression revealed a higher infiltration of T cytotoxic lymphocytes in EBV+ GCLSs, when compared to EBV– GCLSs. Within the eight EBV– cases, which showed a less prominent T-cell inflamed phenotype and lower expression of immune inhibitory molecules, four cases were MSI-high tumors. When EBV+ and MSI-high molecular GCLSs were compared, the differential expression of immune-related genes was still statistically significant (data not shown). Several studies verified that mismatch-repair deficient tumors exhibit an active Th1/cytotoxic immune microenvironment, high expression of checkpoint molecules and represent the most sensitive molecular subtype to immune checkpoint blockade [19, 49]. The results of this study, although limited to a relative small number of EBV+ GCLS cases, suggest that they may represent, especially in the framework of high lymphocytic infiltrates, an additional predictive molecular subtype for target immunotherapies. In a previous study, Derks et al. [31] studied the transcriptional landscape of EBV+ ( $n = 12$ ) and EBV– ( $n = 10$ ) GCs from the TCGA study, and found a similar gene signature (*IFN $\gamma$* , *CXCL9*, *CXCL10*, *CXCL11*, *IDO*, *GZMB*) in both EBV+ and MSI-high GCs. The study of additional and larger cohorts will be necessary to explore in-depth such preliminary data, for future applications in clinical practice.

We also investigated if *PD-L1* gene amplification could be one of the mechanisms implicated in PD-L1 expression in GCLS. Two main mechanisms are involved in the regulation of PD-L1 expression: innate and adaptive immune response.

The former explains aberrant PD-L1 expression through oncogenic signaling, such as *PD-L1* amplification, disruption of *PD-L1* 3'-UTR and activation of PI3K and MAPK pathways [16, 50–52]. The adaptive immune response consists of induction of PD-L1 expression, both in tumor and stromal immune cells, by local inflammatory signals, such as the release of INF $\gamma$  by CD8+ TILs [53, 54]. In the present study, the results for *PD-L1* CNA led to the identification of three cases with *PD-L1* amplification, along with high PD-L1 protein and gene expression. Other three cases displayed IRS > 2 in the absence of *PD-L1* amplification, as previously described in GC cases [27, 31] and in keeping with alternative mechanisms driving PD-L1 expression as described above.

In conclusion, this study provided interesting novel insights into the immunological profile of GCLS. First, we confirmed previous findings on the distinctive biological behavior and clinicopathological profile of GCLS and highlighted the role of histopathological analysis in the identification of this rare GC variant. Second, we confirmed the enrichment of EBV+ molecular subtype in GCLS and the mutual exclusivity of EBV+ and MSI-high status. Third, the in-depth characterization of the tumor microenvironment, by digital analysis of immune biomarkers and mRNA expression profiling, revealed that GCLS is characterized by an “inflamed” tumor microenvironment, enriched in T lymphocytes, particularly at the IF of the tumor and in EBV+ cases; moreover, the molecular subgroup of EBV+ tumors showed higher expression of genes related to Th1/cytotoxic and immunosuppressive biomarkers. Fourth, we demonstrated that GCLS frequently displays high PD-L1 protein and mRNA expression, characteristically restricted to EBV+ and MSI-high tumors, and that *PD-L1* amplification plays a putative causative role in a fraction of cases. Therefore, this study highlights the role of EBV infection in promoting an inflamed tumor microenvironment that, according to recent evidence, may be a potential predictive biomarker of response to targeted immunotherapies.

**Acknowledgements** This study was distinguished with the George Tiniaikos Award (28th European Congress of Pathology held in Cologne, Germany).

**Funding** This article is a result of the projects DOCnet (NORTE-01-0145-FEDER-000003/000029), supported by Norte Portugal Regional Operational Programme (NORTE 2020), under the PORTUGAL 2020 Partnership Agreement, through the European Regional Development Fund (ERDF). We thank the support of the following entities/projects: FEDER-Fundo Europeu de Desenvolvimento Regional (COMPETE 2020-Operacional Programme for Competitiveness and Internationalization-POCI), Portugal 2020; FCT-Foundation for Science and Technology/Ministério da Ciência, Tecnologia e Inovação: POCI-01-0145-FEDER-007274; PTDC/BIM-MEC/2834/2014; salary support to GMA: POPH-QREN Type 4.2, European Social Fund and Portuguese Ministry of Science and Technology (MCTES), Contrato Programa no âmbito do Programa Investigador FCT 2013, Ref: IF/00615/2013;

Ph.D. fellowships SFRH/BD/81103/2011; PostDoc FCT fellowship SFRH/BPD/89764/2012 (PO).

## Compliance with ethical standards

**Conflict of interest** The authors declare that they have no conflict of interest.

**Ethical standards** All procedures followed were in accordance with the ethical standards of the responsible committee on human experimentation (institutional and national) and with the Helsinki Declaration of 1964 and later versions.

**Informed consent** This was a retrospective study and, accordingly, the authors were not expected to have consent to participate. Ethics approval was obtained (CES 236-14). No potentially identifiable patient images or data were included in this study.

## References

1. Ferlay J, Soerjomataram I, Ervik M, Dikshit R, Eser S, Mathers C, et al. GLOBOCAN 2012 v1.0, Cancer Incidence and Mortality Worldwide: IARC CancerBase No. 11 [Internet]. Lyon: International Agency for Research on Cancer; 2013. 2012. <http://www.globocan.iarc.fr>. Accessed 01 Feb 2017.
2. Tan IB, Ivanova T, Lim KH, Ong CW, Deng N, Lee J, et al. Intrinsic subtypes of gastric cancer, based on gene expression pattern, predict survival and respond differently to chemotherapy. *Gastroenterology*. 2011;141(2):476–85. <https://doi.org/10.1053/j.gastro.2011.04.042>.
3. Duraes C, Almeida GM, Seruca R, Oliveira C, Carneiro F. Biomarkers for gastric cancer: prognostic, predictive or targets of therapy? *Virchows Arch*. 2014;464(3):367–78. <https://doi.org/10.1007/s00428-013-1533-y>.
4. Bang YJ, Van Cutsem E, Feyereislova A, Chung HC, Shen L, Sawaki A, et al. Trastuzumab in combination with chemotherapy versus chemotherapy alone for treatment of HER2-positive advanced gastric or gastro-oesophageal junction cancer (ToGA): a phase 3, open-label, randomised controlled trial. *Lancet*. 2010;376(9742):687–97. [https://doi.org/10.1016/s0140-6736\(10\)61121-x](https://doi.org/10.1016/s0140-6736(10)61121-x).
5. Fuchs CS, Tomasek J, Yong CJ, Dumitru F, Passalacqua R, Goswami C, et al. Ramucirumab monotherapy for previously treated advanced gastric or gastro-oesophageal junction adenocarcinoma (REGARD): an international, randomised, multicentre, placebo-controlled, phase 3 trial. *Lancet*. 2014;383(9911):31–9. [https://doi.org/10.1016/s0140-6736\(13\)61719-5](https://doi.org/10.1016/s0140-6736(13)61719-5).
6. Wilke H, Muro K, Van Cutsem E, Oh SC, Bodoky G, Shimada Y, et al. Ramucirumab plus paclitaxel versus placebo plus paclitaxel in patients with previously treated advanced gastric or gastro-oesophageal junction adenocarcinoma (RAINBOW): a double-blind, randomised phase 3 trial. *Lancet Oncol*. 2014;15(11):1224–35. [https://doi.org/10.1016/s1470-2045\(14\)70420-6](https://doi.org/10.1016/s1470-2045(14)70420-6).
7. Ralph C, Elkord E, Burt DJ, O'Dwyer JF, Austin EB, Stern PL, et al. Modulation of lymphocyte regulation for cancer therapy: a phase II trial of tremelimumab in advanced gastric and esophageal adenocarcinoma. *Clin Cancer Res Off J Am Assoc Cancer Res*. 2010;16(5):1662–72. <https://doi.org/10.1158/1078-0432.ccr-09-2870>.
8. Muro K, Chung HC, Shankaran V, Geva R, Catenacci D, Gupta S, et al. Pembrolizumab for patients with PD-L1-positive advanced gastric cancer (KEYNOTE-012): a multicentre,

- open-label, phase 1b trial. *Lancet Oncol.* 2016;17(6):717–26. [https://doi.org/10.1016/s1470-2045\(16\)00175-3](https://doi.org/10.1016/s1470-2045(16)00175-3).
9. Moehler M, Delic M, Goepfert K, Aust D, Grabsch HI, Halama N, et al. Immunotherapy in gastrointestinal cancer: recent results, current studies and future perspectives. *Eur J Cancer.* 2016;59:160–70. <https://doi.org/10.1016/j.ejca.2016.02.020>.
  10. Topalian SL, Hodi FS, Brahmer JR, Gettinger SN, Smith DC, McDermott DF, et al. Safety, activity, and immune correlates of anti-PD-1 antibody in cancer. *N Engl J Med.* 2012;366(26):2443–54. <https://doi.org/10.1056/NEJMoa1200690>.
  11. Bilgin B, Sendur MA, Bulent Akinci M, Sener Dede D, Yalcin B. Targeting the PD-1 pathway: a new hope for gastrointestinal cancers. *Curr Med Res Opin.* 2017:1–11. <https://doi.org/10.1080/03007995.2017.1279132>.
  12. FDA approves Merck's KEYTRUDA® (pembrolizumab) for previously treated patients with recurrent locally advanced or metastatic gastric or gastroesophageal junction cancer whose tumors express PD-L1 (CPS greater than or equal to 1). Merck. 2017. <http://bit.ly/2wberGs>. Accessed 5 May 2018.
  13. Fuchs CS, Doi T, Jang RW-J, Muro K, Satoh T, Machado M, et al. KEYNOTE-059 cohort 1: Efficacy and safety of pembrolizumab (pembro) monotherapy in patients with previously treated advanced gastric cancer. *J Clin Oncol.* 2017;35(15\_suppl):4003. [https://doi.org/10.1200/JCO.2017.35.15\\_suppl.4003](https://doi.org/10.1200/JCO.2017.35.15_suppl.4003).
  14. FDA grants accelerated approval to pembrolizumab for tissue/site agnostic indication. US FDA web site. 2017. <https://www.fda.gov/drugs/informationondrugs/approveddrugs/ucm560040.htm>. Accessed 5 May 2018.
  15. Baraniskin A, Van Laethem JL, Wyrwicz L, Guller U, Wasan HS, Matysiak-Budnik T, et al. Clinical relevance of molecular diagnostics in gastrointestinal (GI) cancer: European Society of Digestive Oncology (ESDO) expert discussion and recommendations from the 17th European Society for Medical Oncology (ESMO)/World Congress on Gastrointestinal Cancer, Barcelona. *Eur J Cancer.* 2017;86:305–17. <https://doi.org/10.1016/j.ejca.2017.09.021>.
  16. TCGA. Comprehensive molecular characterization of gastric adenocarcinoma. *Nature.* 2014;513(7517):202–9. <https://doi.org/10.1038/nature13480>.
  17. Saito R, Abe H, Kunita A, Yamashita H, Seto Y, Fukayama M. Overexpression and gene amplification of PD-L1 in cancer cells and PD-L1+ immune cells in Epstein–Barr virus-associated gastric cancer: the prognostic implications. *Mod Pathol.* 2016;30(3):427–39. <https://doi.org/10.1038/modpathol.2016.202>.
  18. Su S, Zou Z, Chen F, Ding N, Du J, Shao J, et al. CRISPR-Cas9-mediated disruption of PD-1 on human T cells for adoptive cellular therapies of EBV positive gastric cancer. *Oncoimmunology.* 2017;6(1):e1249558. <https://doi.org/10.1080/2162402x.2016.1249558>.
  19. Le DT, Durham JN, Smith KN, Wang H, Bartlett BR, Aulakh LK, et al. Mismatch repair deficiency predicts response of solid tumors to PD-1 blockade. *Science.* 2017;357(6349):409–13. <https://doi.org/10.1126/science.aan6733>.
  20. Solcia E, Klersy C, Mastracci L, Alberizzi P, Candusso ME, Diegoli M, et al. A combined histologic and molecular approach identifies three groups of gastric cancer with different prognosis. *Virchows Arch.* 2009;455(3):197–211. <https://doi.org/10.1007/s00428-009-0813-z>.
  21. Grogg KL, Lohse CM, Pankratz VS, Halling KC, Smyrk TC. Lymphocyte-rich gastric cancer: associations with Epstein–Barr virus, microsatellite instability, histology, and survival. *Mod Pathol.* 2003;16(7):641–51. <https://doi.org/10.1097/01.mp.0000076980.73826.c0>.
  22. Shinozaki-Ushiku A, Kunita A, Fukayama M. Update on Epstein–Barr virus and gastric cancer (review). *Int J Oncol.* 2015;46(4):1421–34. <https://doi.org/10.3892/ijo.2015.2856>.
  23. Wang HH, Wu MS, Shun CT, Wang HP, Lin CC, Lin JT. Lymphoepithelioma-like carcinoma of the stomach: a subset of gastric carcinoma with distinct clinicopathological features and high prevalence of Epstein–Barr virus infection. *Hepato-gastroenterology.* 1999;46(26):1214–9.
  24. Lu BJ, Lai M, Cheng L, Xu JY, Huang Q. Gastric medullary carcinoma, a distinct entity associated with microsatellite instability-H, prominent intraepithelial lymphocytes and improved prognosis. *Histopathology.* 2004;45(5):485–92. <https://doi.org/10.1111/j.1365-2559.2004.01998.x>.
  25. Watanabe H, Enjoji M, Imai T. Gastric carcinoma with lymphoid stroma. Its morphologic characteristics and prognostic correlations. *Cancer.* 1976;38(1):232–43.
  26. Bosman FT, Carneiro F, Hruban RH, Theise ND. WHO classification of tumours of the digestive system. Lyon: International Agency for Research on Cancer; 2010.
  27. Dai C, Geng R, Wang C, Wong A, Qing M, Hu J, et al. Concordance of immune checkpoints within tumor immune contexture and their prognostic significance in gastric cancer. *Mol Oncol.* 2016;10(10):1551–8. <https://doi.org/10.1016/j.molonc.2016.09.004>.
  28. Kawazoe A, Kuwata T, Kuboki Y, Shitara K, Nagatsuma AK, Aizawa M, et al. Clinicopathological features of programmed death ligand 1 expression with tumor-infiltrating lymphocyte, mismatch repair, and Epstein–Barr virus status in a large cohort of gastric cancer patients. *Gastric Cancer (Serial Online).* 2016. <https://doi.org/10.1007/s10120-016-0631-3>. <http://link.springer.com>. Accessed 9 Apr 2017.
  29. Li Z, Lai Y, Sun L, Zhang X, Liu R, Feng G, et al. PD-L1 expression is associated with massive lymphocyte infiltration and histology in gastric cancer. *Hum Pathol.* 2016;55:182–89. <https://doi.org/10.1016/j.humpath.2016.05.012>.
  30. Thompson ED, Zahurak M, Murphy A, Cornish T, Cuka N, Abdelfatah E, et al. Patterns of PD-L1 expression and CD8 T cell infiltration in gastric adenocarcinomas and associated immune stroma. *Gut.* 2017;66(5):794–801. <https://doi.org/10.1136/gutjnl-2015-310839>.
  31. Derks S, Liao X, Chiaravalli AM, Xu X, Camargo MC, Solcia E, et al. Abundant PD-L1 expression in Epstein–Barr virus-infected gastric cancers. *Oncotarget.* 2016;7(22):32925–32. <https://doi.org/10.18632/oncotarget.9076>.
  32. Dong M, Wang HY, Zhao XX, Chen JN, Zhang YW, Huang Y, et al. Expression and prognostic roles of PIK3CA, JAK2, PD-L1, and PD-L2 in Epstein–Barr virus-associated gastric carcinoma. *Hum Pathol.* 2016;53:25–34. <https://doi.org/10.1016/j.humpath.2016.02.007>.
  33. Ma C, Patel K, Singhi AD, Ren B, Zhu B, Shaikh F, et al. Programmed death-ligand 1 expression is common in gastric cancer associated with Epstein–Barr virus or microsatellite instability. *Am J Surg Pathol.* 2016;40(11):1496–506. <https://doi.org/10.1097/pas.0000000000000698>.
  34. Boger C, Behrens HM, Mathiak M, Kruger S, Kalthoff H, Rocken C. PD-L1 is an independent prognostic predictor in gastric cancer of western patients. *Oncotarget.* 2016;7(17):24269–83. <https://doi.org/10.18632/oncotarget.8169>.
  35. Setia N, Agoston AT, Han HS, Mullen JT, Duda DG, Clark JW, et al. A protein and mRNA expression-based classification of gastric cancer. *Mod Pathol.* 2016;29(7):772–84. <https://doi.org/10.1038/modpathol.2016.55>.
  36. Das K, Chan XB, Epstein D, Teh BT, Kim K-M, Kim ST, et al. NanoString expression profiling identifies candidate biomarkers of RAD001 response in metastatic gastric cancer. *ESMO Open.* 2016;1(1):e000009. <https://doi.org/10.1136/esmoopen-2015-000009>.

37. R Core Team (2013). R: a language and environment for statistical computing. Vienna, Austria : the R Foundation for Statistical Computing. <http://www.R-project.org/>. Accessed 5 May 2018.
38. Chen DS, Mellman I. Elements of cancer immunity and the cancer-immune set point. *Nature*. 2017;541(7637):321–30. <https://doi.org/10.1038/nature21349>.
39. Park S, Choi MG, Kim KM, Kim HS, Jung SH, Lee JH, et al. Lymphoepithelioma-like carcinoma: a distinct type of gastric cancer. *J Surg Res*. 2015;194(2):458–63. <https://doi.org/10.1016/j.jss.2014.12.005>.
40. Cheng N, Hui DY, Liu Y, Zhang NN, Jiang Y, Han J, et al. Is gastric lymphoepithelioma-like carcinoma a special subtype of EBV-associated gastric carcinoma? New insight based on clinicopathological features and EBV genome polymorphisms. *Gastric Cancer*. 2015;18(2):246–55. <https://doi.org/10.1007/s10120-014-0376-9>.
41. Ramos M, Pereira MA, Dias AR, Faraj SF, Zilberstein B, Cecconello I, et al. Lymphoepithelioma-like gastric carcinoma: clinicopathological characteristics and infection status. *J Surg Res*. 2017;210:159–68. <https://doi.org/10.1016/j.jss.2016.11.012>.
42. Fridman WH, Pages F, Sautes-Fridman C, Galon J. The immune contexture in human tumours: impact on clinical outcome. *Nat Rev Cancer*. 2012;12(4):298–306. <https://doi.org/10.1038/nrc3245>.
43. Lim H, Park YS, Lee JH, Son da H, Ahn JY, Choi KS, et al. Features of gastric carcinoma with lymphoid stroma associated with Epstein–Barr virus. *Clin Gastroenterol Hepatol*. 2015;13(10):1738–44. <https://doi.org/10.1016/j.cgh.2015.04.015>.
44. Chang MS, Kim WH, Kim CW, Kim YI. Epstein–Barr virus in gastric carcinomas with lymphoid stroma. *Histopathology*. 2000;37(4):309–15.
45. Chiaravalli AM, Cornaggia M, Furlan D, Capella C, Fiocca R, Tagliabue G, et al. The role of histological investigation in prognostic evaluation of advanced gastric cancer. Analysis of histological structure and molecular changes compared with invasive pattern and stage. *Virchows Arch*. 2001;439(2):158–69.
46. Fukayama M, Ushiku T. Epstein–Barr virus-associated gastric carcinoma. *Pathol Res Pract*. 2011;207(9):529–37. <https://doi.org/10.1016/j.prp.2011.07.004>.
47. Sohn BH, Hwang JE, Jang HJ, Lee HS, Oh SC, Shim JJ, et al. Clinical significance of four molecular subtypes of gastric cancer identified by The Cancer Genome Atlas Project. *Clin Cancer Res Off J Am Assoc Cancer Res*. 2017. <https://doi.org/10.1158/1078-0432.ccr-16-2211>.
48. Park C, Cho J, Lee J, Kang SY, An JY, Choi MG, et al. Host immune response index in gastric cancer identified by comprehensive analyses of tumor immunity. *Oncoimmunology*. 2017;6(11):e1356150. <https://doi.org/10.1080/2162402x.2017.1356150>.
49. Lloca NJ, Cruise M, Tam A, Wicks EC, Hechenbleikner EM, Taube JM, et al. The vigorous immune microenvironment of microsatellite instable colon cancer is balanced by multiple counter-inhibitory checkpoints. *Cancer Discov*. 2015;5(1):43–51. <https://doi.org/10.1158/2159-8290.cd-14-0863>.
50. Wang W, Sun J, Li F, Li R, Gu Y, Liu C, et al. A frequent somatic mutation in CD274 3'-UTR leads to protein over-expression in gastric cancer by disrupting miR-570 binding. *Hum Mutat*. 2012;33(3):480–4. <https://doi.org/10.1002/humu.22014>.
51. Wang W, Li F, Mao Y, Zhou H, Sun J, Li R, et al. A miR-570 binding site polymorphism in the B7-H1 gene is associated with the risk of gastric adenocarcinoma. *Hum Genet*. 2013;132(6):641–8. <https://doi.org/10.1007/s00439-013-1275-6>.
52. Kataoka K, Shiraishi Y, Takeda Y, Sakata S, Matsumoto M, Nagano S, et al. Aberrant PD-L1 expression through 3'-UTR disruption in multiple cancers. *Nature*. 2016;534(7607):402–6. <https://doi.org/10.1038/nature18294>.
53. Boussiotis VA. Molecular and biochemical aspects of the PD-1 checkpoint pathway. *N Engl J Med*. 2016;375(18):1767–78. <https://doi.org/10.1056/NEJMra1514296>.
54. Spranger S, Spaepen RM, Zha Y, Williams J, Meng Y, Ha TT, et al. Up-regulation of PD-L1, IDO, and T(regs) in the melanoma tumor microenvironment is driven by CD8(+) T cells. *Sci Transl Med*. 2013;5(200):200ra116. <https://doi.org/10.1126/scitranslmed.3006504>.

## Affiliations

Irene Gullo<sup>1,2,3,4</sup> · Patrícia Oliveira<sup>3,4</sup> · Maria Athelougou<sup>5</sup> · Gilza Gonçalves<sup>2,3,4,6</sup> · Marta L. Pinto<sup>4,7,8</sup> · Joana Carvalho<sup>3,4</sup> · Ana Valente<sup>3,4</sup> · Hugo Pinheiro<sup>3,4,9</sup> · Sara Andrade<sup>3,4,10</sup> · Gabriela M. Almeida<sup>3,4</sup> · Ralf Huss<sup>5</sup> · Kakoli Das<sup>11</sup> · Patrick Tan<sup>11,12,13</sup> · José C. Machado<sup>2,3,4</sup> · Carla Oliveira<sup>2,3,4</sup> · Fátima Carneiro<sup>1,2,3,4</sup> 

<sup>1</sup> Department of Pathology, Centro Hospitalar de São João, Al. Prof. Hernâni Monteiro 4200-319 Porto, Portugal

<sup>2</sup> Department of Pathology, Faculty of Medicine of the University of Porto (FMUP), Al. Prof. Hernâni Monteiro 4200-319 Porto, Portugal

<sup>3</sup> Institute of Molecular Pathology and Immunology at the University of Porto (Ipatimup), Rua Júlio Amaral de Carvalho 45, 4200-135 Porto, Portugal

<sup>4</sup> Instituto de Investigação e Inovação em Saúde (i3S), University of Porto, Rua Alfredo Allen 208 4200-135 Porto, Portugal

<sup>5</sup> Definiens AG, Bernhard-Wicki Str 5 80636 Munich, Germany

<sup>6</sup> Department of Biomedical Sciences and Medicine, University of Algarve, Campus De Gambelas 8005-139 Faro, Portugal

<sup>7</sup> INEB-Institute of Biomedical Engineering, University of Porto, Rua Alfredo Allen 208 4200-135 Porto, Portugal

<sup>8</sup> ICBAS-Institute of Biomedical Sciences Abel Salazar, University of Porto, Rua Jorge De Viterbo Ferreira 228 4050-343 Porto, Portugal

<sup>9</sup> Hospital Senhora da Oliveira, Rua Dos Cutileiros 114 4835-044 Guimarães, Portugal

<sup>10</sup> Department of Biomedicine, Faculty of Medicine of the University of Porto (FMUP), Al. Prof. Hernâni Monteiro 4200-319 Porto, Portugal

<sup>11</sup> Cancer and Stem Cell Biology Program, Duke-NUS Medical School, 8 College Road, Singapore 169857, Singapore

<sup>12</sup> Genome Institute of Singapore, Biopolis, 60 Biopolis St, Singapore 138672, Singapore

<sup>13</sup> Cancer Science Institute of Singapore, National University of Singapore, 14 Medical Dr, Singapore 117599, Singapore